

Fermion mediated pairing in the Ruderman-Kittel-Kasuya-Yosida to Efimov transition regime

Geyue Cai, Henry Ando, Sarah McCusker, and Cheng Chin
*The James Franck Institute, Enrico Fermi Institute, and Department of Physics,
 The University of Chicago, Chicago, IL 60637, USA*

The Ruderman-Kittel-Kasuya-Yoshida (RKKY) interaction and Efimov physics are two distinct quantum phenomena in condensed matter and nuclear physics, respectively. The RKKY interaction describes correlations between impurities mediated by an electron gas, while Efimov physics describes universal bound states of three particles with resonant interactions. Recently, both effects have been observed in Bose-Fermi mixtures in the weak and resonant interaction regimes, respectively. Intriguing conjectures exist to elucidate how the two phenomena meet in the transition regime where the mixture is strongly interacting. In this work, we explore the RKKY-Efimov transition in a mixture of bosonic ^{133}Cs and fermionic ^6Li near a tunable interspecies Feshbach resonance. From dispersion and relaxation measurements, we find that the transition is highlighted by a fermion-mediated scattering resonance between Cs atoms and a weaker resonance on Li atoms. These resonances represent reactive scattering of Cs and Li atoms in the many-body regime, which reduces to an Efimov resonance in the thermal gas regime. Our observation demonstrates the intriguing interplay of two-, three-, and many-body physics in an Bose-Fermi mixture that connects condensed matter physics, nuclear physics and quantum many-body chemistry.

Ultracold atoms offer a powerful platform to explore exotic quantum phases and quantum dynamics that are conjectured across physics disciplines ranging from condensed matter, to nuclear, to cosmological physics [1]. A unique advantage of cold atoms is their tunable interactions through Feshbach resonances [2], permitting precise and smooth tuning of the system from weak to strong interaction regime. Emergent phenomena, phase transitions, and novel quantum dynamics can thus be experimentally identified and compared with theoretical prediction in great details [3].

Among the modern approaches to control atomic interactions, one promising development to engineer long-range potentials is based on mixtures of different atomic species. In cold atom mixtures, interactions between one species mediated by the other species have been demonstrated experimentally [4–8], and offer great flexibility to control the strength and the functional form of the effective potential [9, 10]. Such mediated interactions offer promising perspectives to simulate new classes of quantum systems in nature [11], including long-range interactions between fundamental particles [12], superconducting materials [13], and magnetic orders in materials [14–16].

Mixtures of particles with a large mass imbalance are particularly favorable for studying mediated interactions. The large mass ratio validates the Born-Oppenheimer approximation such that the light, fast moving particles induce an effective potential $V(r)$ between two heavy, slowly moving particles separated by a distance r . Light bosons and heavy fermions, for example, are best to simulate phonon-mediated Cooper pairing in superconductors [17–22]. Meanwhile, a heavy-boson light-fermion mixture can enhance the fermion-mediated interaction. This leads to a strong Efimov potential for boson-boson-fermion three-body systems [23, 24] and RKKY interactions for bosonic impurities embedded in a degenerate

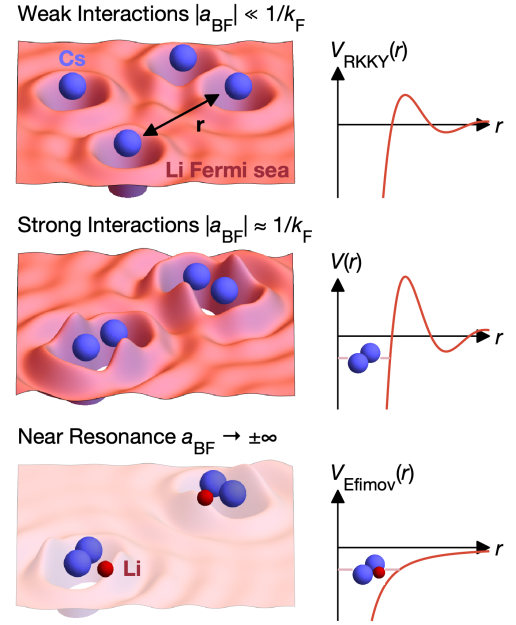


FIG. 1. Quantum mixtures of heavy bosonic ^{133}Cs atoms (blue) and light fermionic ^6Li atoms (red) in different interaction regimes. In the weak coupling regime with small interspecies scattering length $|a_{\text{BF}}| \ll 1/k_F$ (top panel), fermionic scattering leads to interactions between Cs atoms through the Ruderman-Kittel-Kasuya-Yosida (RKKY) mechanism. The RKKY potential $V_{\text{RKKY}}(r)$ shows Friedel oscillations due to fermion scattering (ripples in the Fermi sea) at the Fermi length scale $1/k_F$. In the strong coupling regime $|a_{\text{BF}}| \sim k_F^{-1}$ (middle panel), this paper reports binding of Cs atoms due to enhanced mediated interactions $V(r)$. Near the interspecies Feshbach resonance $a_{\text{BF}} \rightarrow \pm\infty$ (bottom panel), the effective potential supports Efimov Cs_2Li states. Because of the large boson-fermion mass ratio, all effective potentials can be expressed as a function of the bosonic separation r .

Fermi gas [10].

The mixture of bosonic ^{133}Cs and fermionic ^6Li atoms is an excellent platform to probe the above physics. The combination has both a large mass ratio of $m_{\text{Cs}}/m_{\text{Li}} \approx 22.1$ and convenient Feshbach tuning of the interspecies scattering length a_{BF} [25, 26]. Because of the mass ratio enhancement, multiple Efimov states are observed near Feshbach resonances $a_{\text{BF}} \rightarrow \pm\infty$ [27, 28]. In the weak coupling regime with $|a_{\text{BF}}| \ll k_F^{-1}$, where k_F is the Fermi wavenumber, RKKY-type fermion-mediated interactions between Cs atoms are observed [4, 6]. These works demonstrate the Efimov and RKKY effects in the resonant- and weak-interaction limit, respectively, see Fig. 1.

In the transition regime where RKKY and Efimov physics meet, the Bose-Fermi mixture is strongly interacting with the scattering length comparable with the Fermi length scale $|a_{\text{BF}}| \approx k_F^{-1}$. Novel quantum phenomena are conjectured here, including fermionic zero sound [29], three-body states in the Fermi sea [30, 31], p -wave fermionic superfluidity [21], Bose-Fermi droplets [32], and mediated Cs_3 bound states [33], as well as the decay of the mixture, which may simulate the collapse dynamics of white dwarf stars [34].

In this work, we investigate the Cs-Li quantum mixture in the ‘‘RKKY-Efimov’’ transition regime by tuning the interspecies interactions across a Feshbach resonance. We show that the transition physics is highlighted by a fermion mediated resonance between Cs atoms, when the scattering length approaches the Fermi gas length scale $k_F|a_{\text{BF}}| \approx 1$. Resonant structure manifests in both the dynamical response of collective excitations as well as the decay and heating of the Cs condensate. The resonance position can be compared with theoretical model that incorporates both RKKY and Efimov physics. Our observations offer new insight into different fermion mediated two- and three-body binding processes in the many-body regime.

Our experiments begin with a BEC of 30,000 ^{133}Cs atoms immersed in a single component degenerate Fermi gas of up to 20,000 ^6Li atoms. The mixture is prepared in a single beam dipole trap with a weak axial (x) and tight transverse (y and z) confinement. The trap frequencies are $\omega_{\text{Cs}} = (\omega_x, \omega_y, \omega_z) = 2\pi \times (6.53, 153, 114)$ Hz for Cs and $\omega_{\text{Li}} = 2\pi \times (36, 330, 330)$ Hz for Li. Both species are spin-polarized in their lowest hyperfine ground state, where the interspecies scattering length a_{BF} can be tuned near a Feshbach resonance at 892.65 G [25, 27]. Over this range, a bare Cs BEC is stable with a moderate boson-boson scattering length $a_{\text{BB}} = 270 a_0$ [36], where a_0 is the Bohr radius. A bare Fermi gas is also stable and non-interacting. The mixture is initially prepared with weak attractive interactions at scattering length $a_{\text{BF}} = -300 a_0$ and a temperature of around 30 nK. The BEC chemical potential is $\mu_{\text{B}} = k_{\text{B}} \times 35$ nK, where k_{B} is the Boltzmann constant, and the Fermi energy is up to $E_{\text{F}} = \hbar^2 k_{\text{F}}^2 / 2m = k_{\text{B}} \times 370$ nK, where $2\pi\hbar$ is the Planck constant and m is the fermion mass. See Ref. [6] for

details in the sample preparation.

To probe the mixture in the transition regime, we quickly switch the magnetic field near the Feshbach resonance [35] to vary the interspecies scattering length from weak attraction. We introduce an interaction strength $g = 1,000 a_0/a_{\text{BF}}$ to interpolate the weak coupling RKKY regime $g \ll -1$ and the resonant Efimov regime $g \approx 0$. The RKKY-Efimov transition occurs in our system with $-1 < g \leq 0$, where the mixtures become strongly interacting.

Our first experiment to probe the transition regime is to study the dispersion of the Cs BEC immersed in a Fermi gas. Soon after the magnetic field settles, we imprint a weak periodic phase pattern at spatial frequency k on the sample, leading to the emergence of oscillatory density wave, see Fig. 2. From the *in-situ* images on the Cs BEC, see Figs. 2b and c, we obtain the real and imaginary part of the dispersion $\omega(k)$ from the frequency ω and damping Γ of the density wave response [37]. We perform the experiment for different k , scattering lengths a_{BF} , and Li atom numbers.

In the weak interaction regime $|a_{\text{BF}}| < 500 a_0$, the density wave oscillates with low damping. The measured dispersion $\omega(k)$ can be described by the Bogoliubov dispersion of the BEC with an effective bosonic interactions a_{eff} [4, 6], see Fig. 2d. The extracted a_{eff} is consistent with the RKKY prediction [4] and sound speed measurements [6], see Fig. 2e.

For greater attractions $|a_{\text{BF}}| > 500 a_0$, damping becomes significant. The extracted frequencies and damping rates can be described by the dispersive and absorptive response of a resonance: the frequency first reaches a minimum and then returns to the background value after passing a resonance, where the damping peaks, see Fig. 2f. Near and beyond the Feshbach resonance, the measured frequency deviates from our dispersive model, which we attribute to collision loss and the phase separation in the presence of interspecies repulsion [6]. When we reduce the fermion number, the resonance strength weakens.

To further understand the nature of the resonance, we investigate closely the decay and heating dynamics of Cs BECs embedded in the Fermi gas. Immediately after the magnetic field quench, we monitor the BEC and thermal fractions from the transverse density distribution, see Figs. 3a and 3b. In the weak coupling regime $|a_{\text{BF}}| < 500 a_0$, the BEC remains stable. Near the mediated resonance, however, fast decay of the BEC occurs within milliseconds, accompanied by fast generation of excited atoms. The excitations can be modeled by a Gaussian distribution with an effective temperature $T = 75\text{--}100$ nK. Beyond the mediated resonance, the decay and heating quickly reduce. No discernible resonance features are observed at the positions of Efimov and Feshbach resonances. The fitted resonance positions from Figs. 3c and 3d are consistent with the collective excitation measurement in Fig. 2. The weighted average of the resonance positions from these measurements is

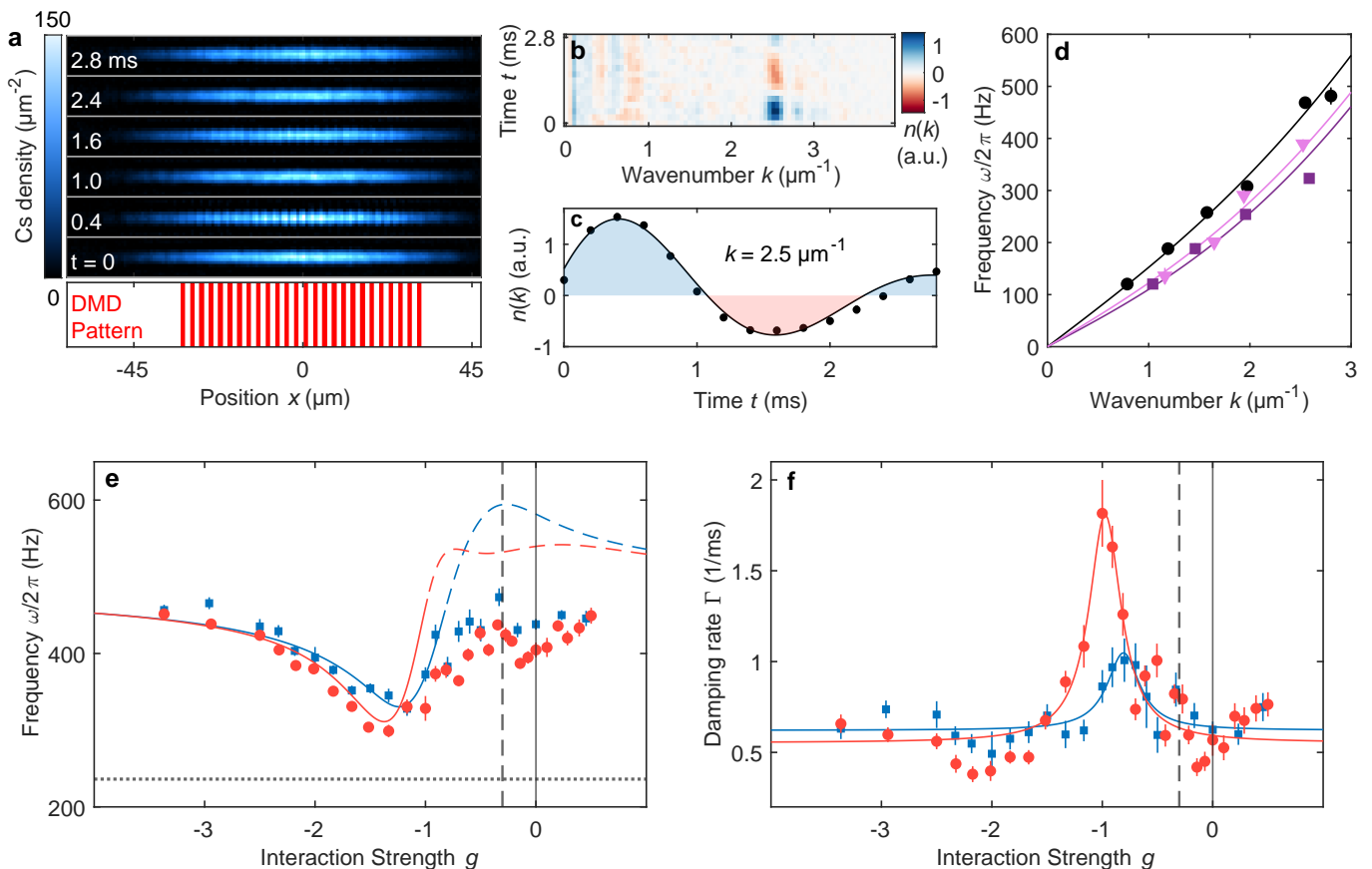


FIG. 2. Dispersion of Cs BEC embedded in a Li degenerate Fermi gas. (a) We imprint a periodic phase on the Cs condensate with a short $80 \mu\text{s}$ pulse of a periodic optical potential, generated by a digital micromirror device (lower panel). The phase modulation at wavenumber $k = 2.5 \mu\text{m}^{-1}$ leads to an oscillating density wave order, shown in *in situ* images of the BECs (upper panel) at an example interspecies scattering length $a_{\text{BF}} = -400 a_0$. (b) Fourier transform of the density profiles $n(k)$. (c) Real part of $n(k)$ is fit to $n = Ae^{-\Gamma t} \sin \omega t$ (solid line), from which we extract the damping Γ , and frequency ω . (d) Measured frequencies ω for $a_{\text{BF}} = -400 a_0$ (black circles), $-688 a_0$ (purple squares), and $a_{\text{BF}} \approx \pm\infty$ (pink triangles). Solid lines are fits to the data based on the Bogoliubov model. (e) Excitation frequency ω and (f) damping Γ at $k = 2.5 \mu\text{m}^{-1}$ show a resonant dispersive and absorptive behavior for samples with 20,000 (red circles) and 10,000 Li atoms (blue squares). Fits based on an empirical model (solid lines), yield resonance positions at $a_{\text{BF}} = -1,030(20) a_0$ for 20,000 Li atoms and $-1,230(50) a_0$ for 10,000 Li atoms. Dashed colored lines in panel (e) indicate the extension of the fit prediction beyond the fitting region, see [35] for more data and analysis. In all panels, error bars are $1\text{-}\sigma$ standard deviations of the mean. In panels (e-f), the black solid line and dashed line indicate the Feshbach resonance and Efimov resonance, respectively. In panel (e), the black dotted line indicates the Cs free particle energy at $k = 2.5 \mu\text{m}^{-1}$.

$a_1 = -1,100(100) a_0$ [35]. The resonance is absent without the degenerate Fermi gas.

We compare the measured resonance position with theoretical models. Calculation based on the RKKY potential shows that the mediated interactions can support a bound state of two impurities at [35]

$$a_{\text{th}} = \frac{\alpha}{k_{\text{F}}^*} \sqrt{\frac{m}{M}} = -1,440 a_0, \quad (1)$$

where m is the mass of the light fermion, M is the mass of the heavy impurity, $\alpha = -2.40\dots$ is a constant, and the wavenumber of the Fermi gas $k_{\text{F}}^* = \eta k_{\text{F}}$ is greater than that of an ideal Fermi gas k_{F} because of the interspecies attraction.

We estimate the enhancement factor $\eta = (1 -$

$g_{\text{BF}} n_{\text{B}} / E_{\text{F}})^{1/2} \approx 2.2$ from the mean-field model, consistent with our independent measurement $\eta = 1.7 \sim 1.9$ [35]. Here n_{B} is the boson density, $g_{\text{BF}} = 2\pi\hbar^2 a_{\text{BF}} / m_{\text{r}}$, and $m_{\text{r}} = Mm / (M + m)$ is the reduced mass of the boson and fermion. An alternative theory that incorporates both the RKKY and the Efimov potentials in the strong coupling regime gives $a_{\text{th}} = -1,600 a_0$ [31, 35]. Both predictions are in fair agreement with our measurement.

The Li Fermi gas behaves differently from the Cs BEC. Near the mediated resonance, Li trap loss is much slower than the BEC damping and decay rates. This supports the picture that Li atoms only “catalyze” the collision resonance between Cs atoms. Pushing to even stronger interspecies attraction, a distinct loss peak appears in the Fermi gas at $a_2 = -1,800(100) a_0$. The resonance is per-

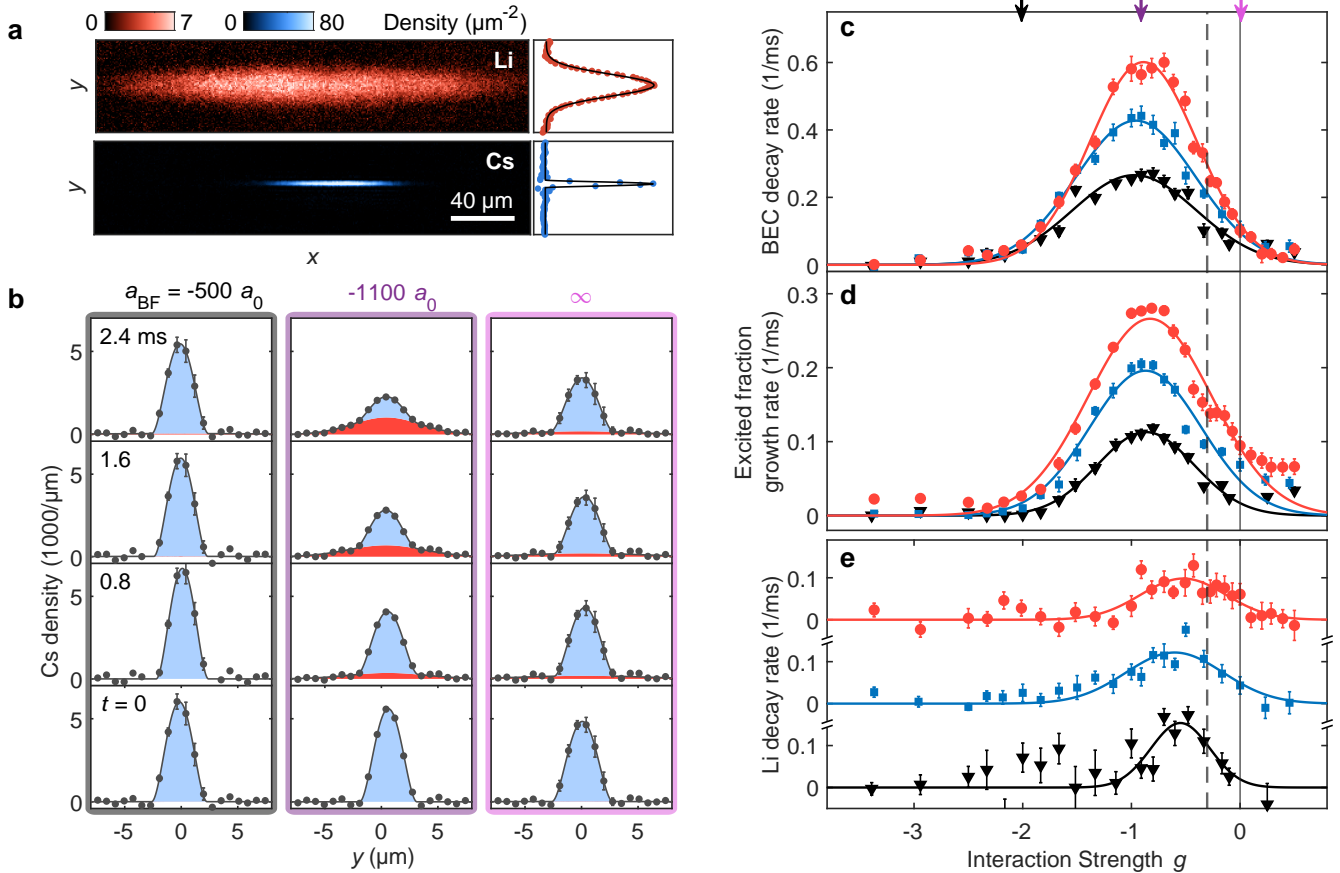


FIG. 3. Resonant decay and excitation Cs BECs induced by the Li degenerate Fermi gas. (a) Example *in-situ* images of Li and Cs. Right panels show axially integrated density profiles. (b) Evolution of Cs density profile below (left), at (middle) and above (right) the mediated resonance at $a_{\text{BF}} = -1, 100 a_0$. Bimodal fits to the density profile show the condensed (blue) and Gaussian (red) parts of the sample. The Gaussian fraction has an effective temperature of 75–100 nK. (c) Cs BEC number decay rate, (d) Cs excited fraction growth rate, and (e) Li number decay rate show resonances for samples with 20,000 (red circles), 10,000 (blue squares), and 5,000 (black triangles) Li atoms. Gaussian fits yield average positions at $a_{\text{BF}} = -1,090(50) a_0$ for the BEC decay, $-1,170(30) a_0$ for the excitation growth, and $-1,800(100) a_0$ for the Li decay. In all panels, error bars are 1- σ standard deviation of the mean. In panels (c-e), the Feshbach resonance (vertical solid line) and Efimov resonance (vertical dashed line) are shown for comparison.

sistent for different fermion densities, and is clearly different from the Efimov resonance at $a_{\text{BF}} = -3,300(240) a_0$ and the Feshbach resonance at $a_{\text{BF}} = \pm\infty$, measured precisely in thermal mixtures of Cs and Li atoms [27].

What is the nature of the two resonances at $a_{\text{BF}} = a_1$ and a_2 in the transition regime, and how are they related to RKKY and Efimov potential? To elucidate the underlying processes, we monitor the resonant features as the mixture is prepared in the classical and quantum regime. Starting with a mixture at the lowest temperature $T \approx 30$ nK, we quickly step up the optical trap intensity to excite the mixture and wait for the mixture to reach a new equilibrium. This process provides precise heating of the sample without discernible trap loss. We then perform trap loss measurement across the resonances, see Fig. 4.

We observe drastic changes in the resonance positions when crossing from the thermal regime into the quan-

tum degeneracy regime. For thermal mixtures above the Cs BEC critical temperature $T > T_c$, both species show resonant features consistent with the Efimov resonance at $a_{\text{BF}} = -3,300 a_0$ and Feshbach resonance $a_{\text{BF}} = \pm\infty$, in agreement with previous works [27]. Below the BEC critical temperature $T < T_c$, the resonances appear at weaker interspecies attraction and a gap between the resonances in the Cs BEC and the Li Fermi gas widens. The result is summarized in Fig. 4b.

Based on our observations, we propose a physical picture to elucidate the impact of quantum degeneracy to the Cs-Li mixtures in the RKKY-Efimov transition regime. As we increase the interspecies attraction from zero, the Fermi gas first mediates bosonic interactions through the RKKY mechanism. When the attraction strengthens and reaches the critical value $a_{\text{BF}} = a_1$ ($-1,100 a_0$ in our system), resonant scattering of bosons occurs, which we denote as a degenerate Fermi gas (DFG)

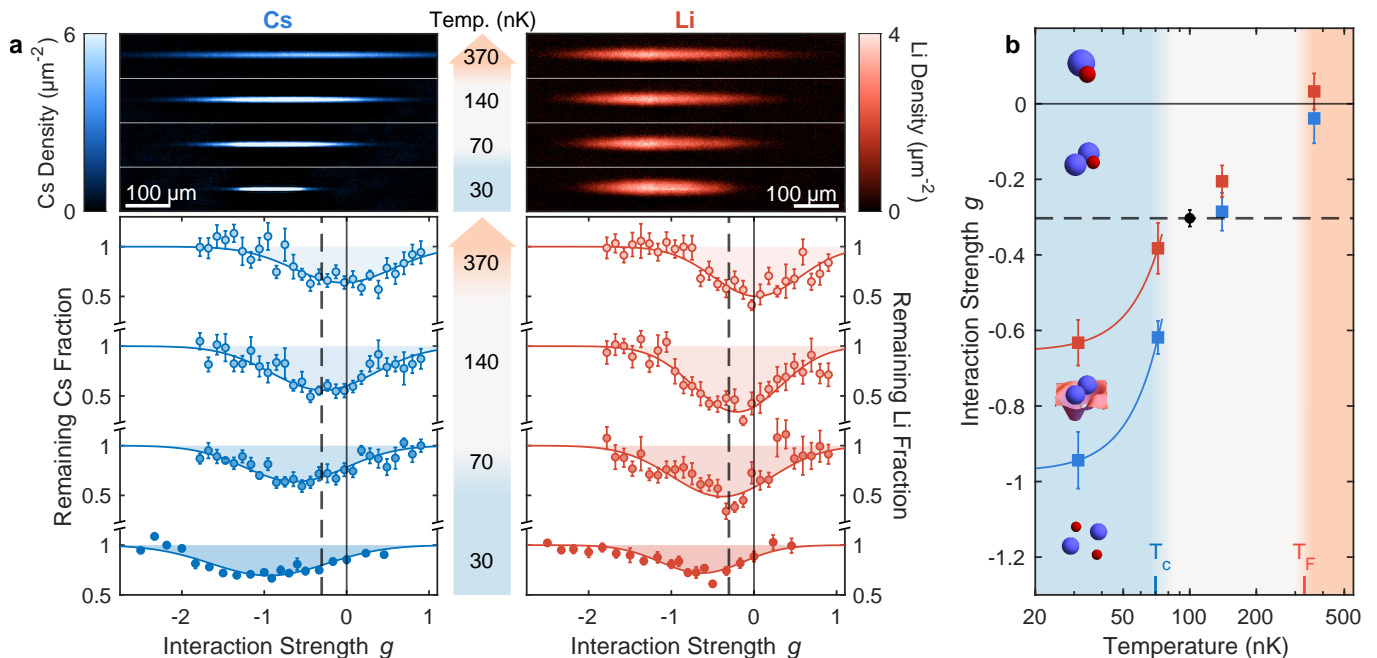
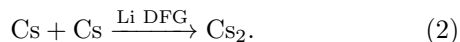


FIG. 4. Fermion mediated resonances in the thermal and quantum regimes. (a) Sample images with 30,000 Cs atoms and 20,000 Li atoms are prepared at 30, 70, 140, and 370 nK. Lower panels show the Cs and Li surviving fraction after hold time $t_h = 2.8, 3, 6,$ and 10 ms for the 30, 70, 140, and 370 nK samples, respectively. We determine the positions of the loss peaks from Gaussian fits (solid lines). (b) Summary of loss centers in the classical and quantum regime. Here $T_c = 75$ nK is the BEC critical temperature, and $T_F = 360$ nK is the Fermi temperature. Li loss centers are shown in red, Cs in blue. The black circle is the measurement from Ref. [27]. Red and blue solid lines are guides to the eye. Cartoons show the hypothesized many-body ground state: free Li (red balls) and Cs atoms (blue balls) for weak attractions $g < -1$, fermion-mediated Cs₂ pairs for $-1 < g < -0.8$ and Cs₂Li trimers for $-0.8 < g < 0$. Finally CsLi dimers form above the Feshbach resonance $g > 1$. In all plots, error bars are $1\text{-}\sigma$ standard deviations of the mean. The solid and dashed lines indicate the Feshbach and the Efimov resonance, respectively.

mediated reaction process:



Enhancing the attraction further brings the system to the second threshold a_2 ($-1,800 a_0$ in our system), where Li atoms are also bound to the boson pairs, denoted as another DFG mediated process:



Both processes in Eqs. (2) and (3) are many-body in nature, discussed in Refs. [31, 33]. When the system enters the normal gas regime, the many-body processes merge into a single three-body process $\text{Cs} + \text{Cs} + \text{Li} \rightarrow \text{Cs}_2\text{Li}$, which is precisely the picture of an Efimov resonance [38].

Our picture offers a consistent understanding of this and previous works [4, 6] on interacting Cs-Li mixtures in all regimes. It also highlights the rich physics of

fermion-mediated binding as a unique feature in the RKKY-Efimov transition regime. The observed smaller bosonic binding length $|a_1|$ and the larger fermionic binding length $|a_2|$ can be understood since heavy particles form a bound state easier than do light particles [35]. This is a trend that persists in the many-body regime, e.g., the mass scaling of Eq. (1) favors pairing of heavier impurities.

We acknowledge T. Enss, V. Galitski and K. Wang for valuable discussions. We thank K. Patel and M. Rautenberg for valuable assistance with the experiment. This work is supported by the National Science Foundation under Grant No. PHY-2409612 and by the Air Force Office of Scientific Research under Award No. FA9550-21-1-0447. H.A. acknowledges support by the National Science Foundation Graduate Research Fellowship under Grant No. DGE 1746045. S.M. acknowledges support by the National Science Foundation under PHY-GRS 2103542.

[1] I. Bloch, J. Dalibard, and S. Nascimbene, Nature Physics 8, 267 (2012).

[2] C. Chin, R. Grimm, P. Julienne, and E. Tiesinga, Rev.

- Mod. Phys. **82**, 1225 (2010).
- [3] E. Altman, K. R. Brown, G. Carleo, L. D. Carr, E. Demler, C. Chin, B. DeMarco, S. E. Economou, M. A. Eriksson, K.-M. C. Fu, M. Greiner, K. R. Hazzard, R. G. Hulet, A. J. Kollár, B. L. Lev, M. D. Lukin, R. Ma, X. Mi, S. Misra, C. Monroe, K. Murch, Z. Nazario, K.-K. Ni, A. C. Potter, P. Roushan, M. Saffman, M. Schleier-Smith, I. Siddiqi, R. Simmonds, M. Singh, I. Spielman, K. Temme, D. S. Weiss, J. Vučković, V. Vuletić, J. Ye, and M. Zwierlein, PRX Quantum **2**, 017003 (2021).
- [4] B. DeSalvo, K. Patel, G. Cai, and C. Chin, Nature **568**, 61 (2019).
- [5] H. Edri, B. Raz, N. Matzliah, N. Davidson, and R. Ozeri, Phys. Rev. Lett. **124**, 163401 (2020).
- [6] K. Patel, G. Cai, H. Ando, and C. Chin, Physical Review Letters **131**, 083003 (2023).
- [7] X.-Y. Chen, M. Duda, A. Schindewolf, R. Bause, I. Bloch, and X.-Y. Luo, Physical Review Letters **128**, 153401 (2022).
- [8] C. Baroni, B. Huang, I. Fritsche, E. Dobler, G. Anich, E. Kirilov, R. Grimm, M. A. Bastarrachea-Magnani, P. Massignan, and G. M. Bruun, Nature Physics **20**, 68 (2024).
- [9] D. Santamore and E. Timmermans, Phys. Rev. A **78**, 013619 (2008).
- [10] S. De and I. B. Spielman, Applied Physics B **114**, 527 (2014).
- [11] R. Paredes, G. Bruun, and A. Camacho-Guardian, Physical Review A **110**, 030101 (2024).
- [12] S. Weinberg, *The quantum theory of fields*, Vol. 2 (Cambridge university press, 1995).
- [13] M. Tinkham, *Introduction to superconductivity*, Vol. 1 (Courier Corporation, 2004).
- [14] M. A. Ruderman and C. Kittel, Phys. Rev. **96**, 99 (1954).
- [15] T. Kasuya, Progress of theoretical physics **16**, 45 (1956).
- [16] K. Yosida, Phys. Rev. **106**, 893 (1957).
- [17] M. J. Bijlsma, B. A. Heringa, and H. T. C. Stoof, Phys. Rev. A **61**, 053601 (2000).
- [18] H. Heiselberg, C. J. Pethick, H. Smith, and L. Viverit, Phys. Rev. Lett. **85**, 2418 (2000).
- [19] L. Viverit, Phys. Rev. A **66**, 023605 (2002).
- [20] F. Matera, Phys. Rev. A **68**, 043624 (2003).
- [21] J. Kinnunen, Z. Wu, and G. M. Bruun, Phys. Rev. Lett. **121**, 253402 (2018).
- [22] D. V. Efremov and L. Viverit, Phys. Rev. B **65**, 134519 (2002).
- [23] V. Efimov, Physics Letters B **33**, 563 (1970).
- [24] P. Naidon and S. Endo, Reports on Progress in Physics **80**, 056001 (2017).
- [25] S. Tung, C. Parker, J. Johansen, C. Chin, Y. Wang, and P. S. Julienne, Phys. Rev. A **87**, 010702(R) (2013).
- [26] M. Repp, R. Pires, J. Ulmanis, R. Heck, E. D. Kuhnle, M. Weidemüller, and E. Tiemann, Physical Review A **87**, 010701 (2013).
- [27] J. Johansen, B. DeSalvo, K. Patel, and C. Chin, Nature Physics **13**, 731 (2017).
- [28] R. Pires, J. Ulmanis, S. Häfner, M. Repp, A. Arias, E. D. Kuhnle, and M. Weidemüller, Physical Review Letters **112**, 250404 (2014).
- [29] X. Shen, N. Davidson, G. M. Bruun, M. Sun, and Z. Wu, Physical Review Letters **132**, 033401 (2024).
- [30] M. Sun and X. Cui, Physical Review A **99**, 060701 (2019).
- [31] T. Enss, B. Tran, M. Rautenberg, M. Gerken, E. Lippi, M. Drescher, B. Zhu, M. Weidemüller, and M. Salmhofer, Phys. Rev. A **102**, 066321 (2020).
- [32] D. Rakshit, T. Karpiuk, M. Brewczyk, and M. Gajda, SciPost Phys. **6**, 079 (2019).
- [33] S. Fisher, O. Ogunnaike, and L. Levitov, Physical Review A **109**, 043323 (2024).
- [34] T. Karpiuk, M. Nikolajuk, M. Gajda, and M. Brewczyk, Sci Rep **11**, 2286 (2021).
- [35] See supplementary materials.
- [36] M. Berninger, A. Zenesini, B. Huang, W. Harm, H.-C. Nägerl, F. Ferlaino, R. Grimm, P. S. Julienne, and J. M. Hutson, Phys. Rev. A **87**, 032517 (2013).
- [37] I. Shammass, S. Rinott, A. Berkovitz, R. Schley, and J. Steinhauer, Physical Review Letters **109**, 195301 (2012).
- [38] T. Kraemer, M. Mark, P. Waldburger, J. G. Danzl, C. Chin, B. Engeser, A. D. Lange, K. Pilch, A. Jaakkola, H.-C. Nägerl, and R. Grimm, Nature **440**, 315 (2006).
- [39] R. Veyron, V. Mancois, J.-B. Gerent, G. Baclet, P. Bouyer, and S. Bernon, Physical Review Research **4**, 033033 (2022).
- [40] C. Pethick and H. Smith, *Bose-Einstein condensation in dilute gases* (Cambridge University Press, 2002).
- [41] G. Kavoulakis and C. J. Pethick, Phys. Rev. A **58**, 1563 (1998).
- [42] V. V. Babikov, Soviet Physics Uspekhi **10**, 271 (1967).

Supplementary Material for Fermion mediated pairing of bosons in the strong coupling regime

Geyue Cai, Henry Ando, Sarah McCusker, and Cheng Chin
The James Franck Institute, Enrico Fermi Institute and Department of Physics,
The University of Chicago, Chicago, IL 60637, USA

A. *In situ* imaging of Li and Cs atoms

New to this work, we have implemented microscope absorption imaging of Li atoms through the same beam path. Moreover, we use the “fast kinetics mode” of our Andor Ikon-M CCD camera to take single-shot images of both species. When imaging Li first, we expose only the top 140 pixels of the CCD to the Li light+atoms pulse, then shift down the stored charges into the dark region before exposing the Cs light+atoms pulse in the top 140 pixels. This continues for the Li light only and Cs light only pulses. The shift time, and thus the time between imaging the two species, is 0.42 ms. This is a short enough time that the heavy Cs atoms should move at most ~ 1 pixel between the Li imaging pulse and the Cs imaging pulse. However, we find that taking Li images first reduces the data quality of the phase imprinting experiments reported in Fig. 2, so for the data in Figs. 2 and 3 we image Cs before Li.

Additionally, we have implemented the high-density absorption imaging calibration [39] for our Cs microscope imaging. We find that this method improves the agreement between our measured Cs density profile and Thomas-Fermi predictions.

B. Phase imprinting experiment

For the data shown in Figs. 2 and 3 (and the 30 nK data in Fig. 4), our experimental procedure is shown in Fig. S2. After preparing a degenerate mixture, we ramp the magnetic field from $a_{\text{BF}} = -150 a_0$ to $-300 a_0$ in 20 ms. After letting the field settle for 5 ms, we apply a carefully engineered field jump sequence which achieves the target magnetic field within 0.8 ms, after which the field is stable within 10 mG. We call the beginning of the field jump $t = -1$ ms.

We apply an 80 μs repulsive DMD pulse at $t = -0.08$ ms, 0.92 ms after initiating the field jump. Ref. [6] contains details of our DMD projection system. The DMD pattern we apply is a simple n -on n -off vertical stripe pattern for the main data in Fig. 2e-f, although for longer wavelength patterns such as those depicted in Fig. 2d, we use a pattern that approximates a sinusoidal intensity using the error diffusion halftoning algorithm, as the simple binary pattern produces noticeable higher spatial harmonics at long wavelengths. By varying the DMD pulse duration, we verified that the measured density wave amplitude is linear in the DMD pulse length, showing that we are not exciting too large a fraction of

the condensate into the $\pm k$ modes.

After applying the DMD pulse, we wait a varying hold time t before taking a Cs-first dual-species *in situ* image (Sec. A). We perform three rounds of the experiment at each scattering length and each value of t for averaging. This raw data is used for both Figs. 2 and 3, but from this point the analyses of Figs. 2 and 3 diverge.

To analyze the quasiparticle dispersion as in Fig. 2, we proceed by integrating along the tight axis of each image to produce a 1D density profile (Fig. S2 continued). We then fit and subtract off a bimodal background distribution separately at each time t to produce a background-free view of the density wave evolution. Next, we Fourier transform the data at each time step, and rotate the phase of the resulting Fourier spectrum $n(k, t)$ so that the datum with the largest amplitude is real and positive (typically, this datum is expected to be at $k = k$ and t slightly greater than 0).

Finally, we perform a 2D fit to the real part of this resulting Fourier transform. The fit function we use is Gaussian in k and an underdamped oscillator in t ,

$$n_{\text{fit}}(k, t) = A e^{-(k-k_0)^2/2\sigma_k^2} e^{-\Gamma t} \sin \omega t, \quad (4)$$

where A, k_0, σ_k, Γ , and ω are fit parameters, and we only use the data from a small region around k for the fit. This model fits the most of the $k = 2.5 \mu\text{m}^{-1}$ data reasonably well, as the density wave appears underdamped in all but the most rapidly decaying condensates (around $a_{\text{BF}} \approx -1,100 a_0$).

In Fig. 2d, we fit Bogliubov dispersion curves

$$\omega(k) = \frac{1}{\hbar} \sqrt{\epsilon_k^2 + 2n_{\text{B}}\alpha a_{\text{eff}}\epsilon_k} \quad (5)$$

to the extracted $\omega(k)$ data to verify the validity of our method, where n_{B} is the average boson density across the condensate, $\epsilon_k = \hbar^2 k^2 / 2M$ is the free particle dispersion, $\alpha = 4\pi\hbar^2 / M$, M is the mass of a Cs atom, and a_{eff} is an fit parameter representing the effective scattering length between bosons [40, 41].

In Fig. 2e-f, we employ an empirical model and a multi-step fitting procedure to fit the data and extract a resonance position. The data in Fig. 2e-f are reproduced in Fig. We assume that the effective boson-boson scattering length \tilde{a}_{eff} may be complex, and takes the form

$$\tilde{a}_{\text{eff}} = a_{\text{BB}} + \frac{\Delta}{1/a_{\text{BF}} - 1/a_{\text{res}} + i\gamma}, \quad (6)$$

where a_{BF} is the boson-fermion scattering length, a_{BB} is the known background boson-boson scattering length,

Measurement	20,000 Li	10,000 Li	5,000 Li	Average
Dispersion (a_0)	-1,030(20)	-1,230(50)	-1,220(90)	-1,100(100)
BEC decay rate (a_0)	-1,120(10)	-1,040(20)	-1,030(30)	-1,090(50)
Excited fraction growth rate (a_0)	-1,210(30)	-1,150(40)	-1,150(30)	-1,170(30)
Li decay rate (a_0)	-1,900(200)	-1,700(200)	-1,800(200)	-1,800(100)

TABLE I. Table of resonance positions extracted from different quantities and different Li numbers in units of a_0 . The Average column denotes a weighted average with error bars from the standard deviation. Centers are extracted from fits in Fig. 2 and 3. The additional 5,000 Li dataset in Fig. S1 is also included. The weighted average and standard deviation of all results for dispersion, BEC decay rate, and excited fraction growth rate are summarized as $a_1 = 1,100(100) a_0$. The weighted average of the Li decay rate resonance positions are summarized as $a_2 = -1,800(100) a_0$.

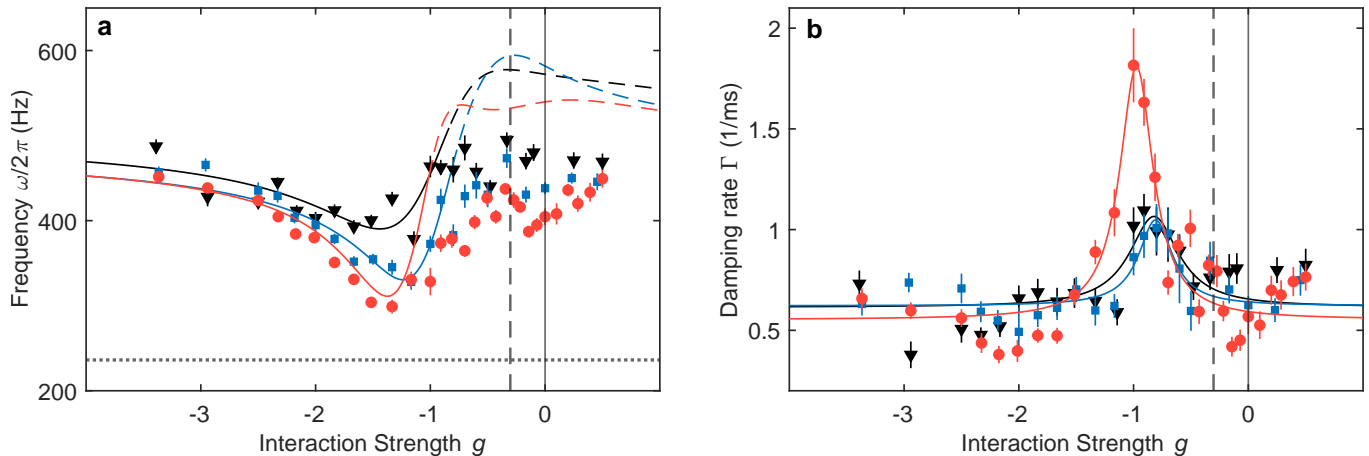


FIG. S1. Dispersion of a Cs BEC embedded in a Li Fermi gas, with an additional dataset relative to Fig. 2. (e) Excitation frequency ω and (f) damping Γ at $k = 2.5 \mu\text{m}^{-1}$ show a resonant dispersive and absorptive behavior respectively, for samples with 20,000 (red circles) and 10,000 (blue squares) and 5,000 (black triangles) Li atoms. Fits based on an empirical model (solid lines), yield resonance positions at $a_{\text{BF}} = -1030(20) a_0$, $1230(50) a_0$, and $1220(90) a_0$ for 20,000, 10,000 and 5,000 Li atoms respectively. Dashed colored lines in panel (e) indicate the extension of the fit prediction beyond the fitting region. In all panels, error bars are $1\text{-}\sigma$ standard deviations of the mean. In both panels the vertical black solid line indicates the Feshbach resonance position, and the black dashed line indicates the Efimov resonance position. In panel (a), the black dotted line indicates the Cs free particle energy at $k = k = 2.5 \mu\text{m}^{-1}$.

and Δ , a_{res} , and γ are unknown parameters having to do with the strength, central position, and dissipativity of the resonance.

Plugging this model into the Bogliubov dispersion Eq. 5 gives

$$\omega + i\Gamma = \sqrt{\epsilon_k^2 + 2n_{\text{B}}\epsilon_k\alpha\tilde{a}_{\text{eff}}}, \quad (7)$$

where Γ is the quasiparticle decay rate and all other quantities are as above. Due to the strong BEC decay we report in Fig. 3, the BEC density n_{B} varies substantially with varying a_{BF} . We thus use a Gaussian fit to the BEC loss to obtain a prediction for the time-averaged BEC density at varying a_{BF} , and use this empirical average density in the fits. Nonetheless, a direct, simultaneous fit of Eq. 7 to the quasiparticle dispersion and damping does not match the data well; the model seems to have too few free parameters.

We therefore adopt a two-step fitting process for the Fig. 2e-f data. First, we fit a Lorentzian to the damping data (Fig. 2f) to extract a resonance position. We then fit the frequency data (Fig. 2e) to the real part of Eq. 7.

This model always predicts both a decrease in ω to the left of resonance and an increase in ω to the right of resonance; however, both datasets in Fig. 2e only show a decrease and not the corresponding increase. We suspect this may be due to strong Li loss from the BEC volume near resonance or some other effect for which we do not yet have a model. Therefore, for Fig. 2e we fit only the ω data to the left of the resonances obtained from the Lorentzian fits in Fig. 2f. In Fig. 2e, we indicate the fit region by solid lines and the unfitted region with dashed lines.

An additional dataset with 5,000 Li atoms is omitted from Fig. 2 for visual clarity, but provided here in Fig. S1. Resonance positions extracted from fits are reported in Table I, which also reports resonance positions from Fig. 3.

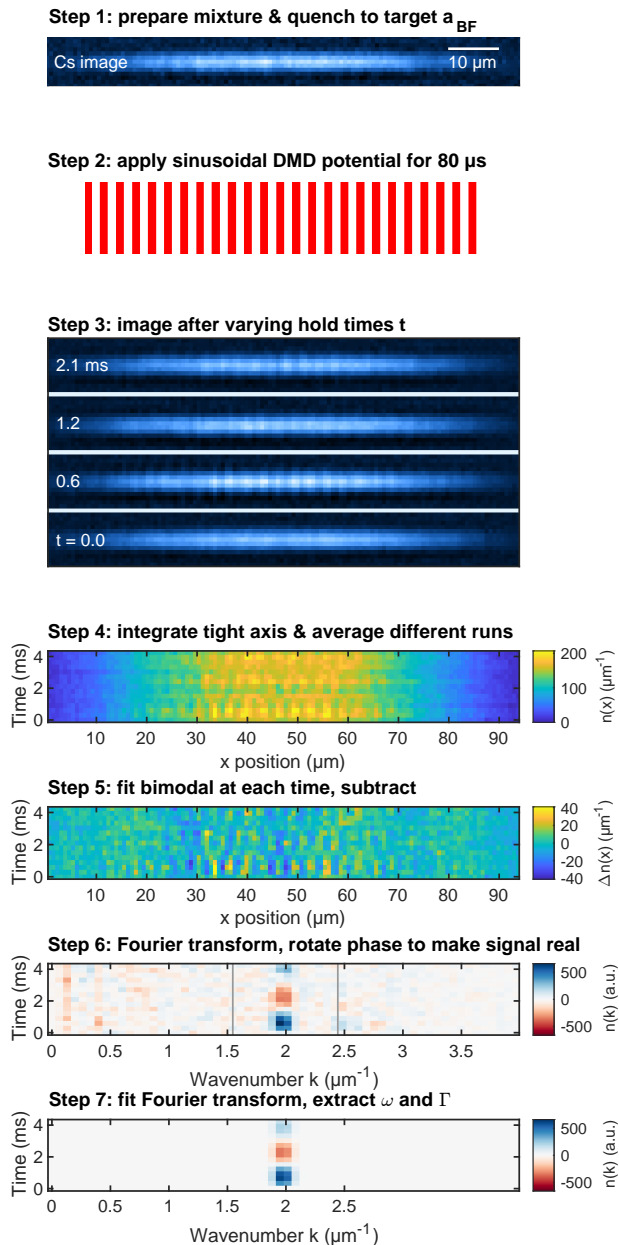


FIG. S2. Our analysis procedure for phase imprinting experiments. In Step 1, we prepare a degenerate ^{133}Cs - ^6Li Bose-Fermi mixture at weak attractive interactions ($a_{\text{BF}} = -300 a_0$), before quenching in 0.8 ms to a target interactions strength. We then apply an $80 \mu\text{s}$ repulsive DMD potential with spatial frequency k to the sample. In Step 3, we then image after varying hold times. In Step 4, we integrate along the radial direction and average the three rounds of data together to get the 1D axial density $n(x)$. In Step 5, we fit a bimodal at each time and subtract off the fit to get a background-free view of the density waves, $\Delta n(x)$. In Step 6, we Fourier transform $\Delta n(x)$, then rotate the phase of the resulting Fourier transform to make the density wave signal real. We call the Fourier transform $n(k)$. The vertical gray lines in Step 6 show the extent of the fit region that we use in Step 7, where we perform a fit as described in Eq. 4 to extract the frequency ω and damping Γ of the density wave oscillations.

C. Preparation of Cs-Li samples at different temperatures

In Fig. 4, we prepare mixtures at varying temperatures. For these experiments, we mostly follow the normal preparation and evaporation procedure of Figs. 2-3, but rather than holding the sample at the lowest trap depth for 500 ms before imaging, we hold the sample at the lowest trap depth for only 200 ms, then heat the mixture by jumping the trap depth to a deeper value before waiting the remaining 300 ms. We find that this 300 ms hold provides enough time for the density profiles of both species to stop changing, and by staying at the deeper trap depth we retain similar atom numbers in both species as compared to the degenerate sample.

We extract the temperature by performing a bimodal fit to the Cs axial density profile. Assuming the axial trap frequency (which mostly comes from magnetic trapping) is still $\omega_x = 2\pi \times 6.53 \text{ Hz}$, the temperature is related to the width σ of the Gaussian part of the bimodal distribution through $k_B T = m_B \omega_x^2 \sigma^2$. To fit the small thermal fraction at 35 nK, we further constrain our fit by enforcing that the condensate fraction $N_0/N = 1 - (T/T_c)^3$, where T_c is the condensation temperature.

Our Fig. 4 analysis procedure is straightforward: we take dual-species *in situ* images at each a_{BF} value and each temperature, fit a bimodal (Gaussian) distribution to the Cs (Li) radial density profile, and extract atom numbers from each. We perform two calibrations as we go. Firstly, after each full data round (each a_{BF} value and each temperature), we perform a magnetic field calibration to determine the electromagnet current corresponding to the magnetic field of the Feshbach resonance. We then interpolate this current-field calibration across the intervening data to get an accurate magnetic field value for each datum, and then bin the data before averaging to get Fig. 4. Secondly, rather than assuming a constant initial Cs and Li number, we take data at both $t = 0$ as well as $t = t_h$, then compensate for systematic differences in initial number by reporting the final / initial number instead of just final number.

D. Li Density Enhancement

To estimate the local enhancement of k_F due to the interspecies attraction, we work within the Thomas-Fermi approximation. Additionally, since the Fermi gas's dynamical time scale (limited by $\hbar/E_F \approx 23 \mu\text{s}$) is much shorter than the time scale of the magnetic field jump (0.8 ms), we expect the Fermi gas is able to follow the magnetic field jump. Thus, after jumping to the new interaction strength g_{BF} , we have

$$E_F = \frac{(\hbar k_F^*)^2}{2m_F} + g_{\text{BF}} n_B + V, \quad (8)$$

where $k_F^* = (6\pi^2 n_F^*)^{1/3}$ is the local fermion wavenumber, n_F^* is the local fermion density modified by the inter-

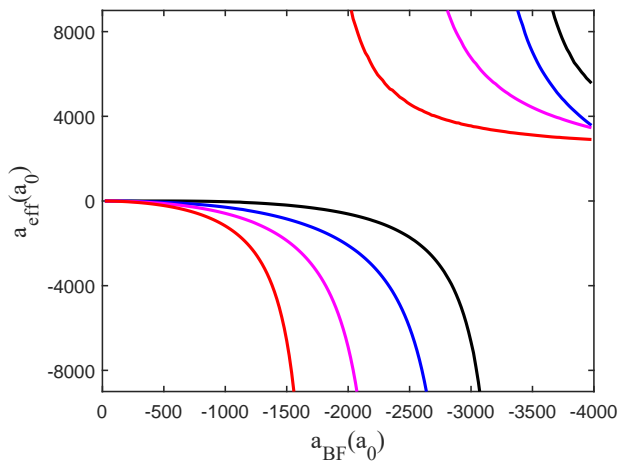


FIG. S3. Effective scattering length between Cs atoms in Li Fermi gas with density ≈ 0 (black), $0.1 n_F$ (blue), n_F (magenta), and $10 n_F$ (red). Here $n_F = 4.7 \times 10^{11} \text{cm}^{-3}$ is the nominal density of a non-interacting Li Fermi gas in our experiment while $10n_F$ is approximately the maximum fermion density on our Cs BEC in the presence of strong interspecies attraction. Divergence of the scattering length shows the pairing resonances shifting from the Efimov resonance at $a_{\text{BF}} = -3,300 a_0$, $-2,980 a_0$, $-2,360 a_0$ to $-1,720 a_0$ with increasing densities. The calculation is based on the model in Ref. [31].

species interaction g_{BF} and V is the external trapping potential. The peak value of the enhanced local Fermi wavenumber k_{F}^* is then

$$k_{\text{F}}^* = \sqrt{\frac{2m_{\text{F}}}{\hbar^2}(E_{\text{F}} - g_{\text{BF}}n_{\text{B}})}, \quad (9)$$

giving an enhancement factor

$$\eta = \frac{k_{\text{F}}^*}{k_{\text{F}}} = \sqrt{1 - g_{\text{BF}}n_{\text{B}}/E_{\text{F}}}. \quad (10)$$

This predicts $\eta \approx 2.2$ near the observed resonance at $a_1 = -1,100 a_0$.

An independent confirmation of the fermi gas density enhancement comes from *in situ* images of Li degenerate Fermi gas. Enhanced Li density within the Cs BEC is observed with large interspecies attraction. A strong enhancement of the fermion density on the Cs BEC of $5 \sim 7$ for $-700 a_0 < a_{\text{BF}} < -1,000 a_0$ is observed, which corresponds to $\eta = 1.7 \sim 1.9$.

E. Resonance position of the fermion-mediated potential

We present two estimations on the resonance position of fermion-mediated interactions in the main text. One is based on the leading order RKKY potential $V_{\text{RKKY}}(r)$ and the second model incorporates both RKKY and Efimov effects in the strong coupling regime, following the calculation in Ref. [31].

Consider two heavy impurities with mass M embedded in a degenerate fermi gas of light atoms with mass $m \ll M$ and Fermi energy $E_{\text{F}} = \hbar^2 k_{\text{F}}^2/2m$. Based on the Born-Oppenheimer approximation, the effective potential between the impurities separated by R is given in the limit of weak interaction $\epsilon = |k_{\text{F}} a_{\text{BF}}| \ll 1$ by

$$V_{\text{RKKY}}(R) = E_{\text{F}} \frac{8\epsilon^2}{\pi} \frac{r \cos r - \sin r}{r^4} + O(\epsilon^3), \quad (11)$$

where $r = 2k_{\text{F}}R$ is the reduced separation.

We describe the wavefunction of two impurities interacting with V_{RKKY} with the Schrodinger's equation

$$\left[-\frac{\hbar^2 \nabla^2}{M} + V_{\text{RKKY}}(R) \right] \psi(R) = E\psi(R), \quad (12)$$

which for strong enough attraction can support a bound state at $E = 0$. The condition for the emergence of the bound state can be estimated by solving the variable phase equation for the scattering length function $a(R)$ [42], which yields

$$\frac{da(R)}{dR} = -\frac{M}{\hbar^2} V_{\text{RKKY}}(R) [R - a(R)]^2. \quad (13)$$

We can then calculate the scattering length $a_{\text{eff}} = \lim_{R \rightarrow \infty} a(R)$, and the bound state emerges when the scattering length diverges $a_{\text{eff}} \rightarrow -\infty$.

Integrating the variable phase equation numerically with the RKKY potential up to leading order in ϵ , we obtain the condition on the fermion mediated binding as

$$k_{\text{F}} a_{\text{th}} = -2.40 \dots \sqrt{\frac{m}{M}}. \quad (14)$$

Remarkably, in systems with a large mass ratio $M/m \rightarrow \infty$, impurity binding occurs in the perturbation regime with $|k_{\text{F}} a_{\text{BF}}| \ll 1$, which validates the calculation based on the leading order RKKY potential. Here a_{th} should be compared with a_1 in our experiment.

Our second estimation is based on the calculation that takes both the RKKY and the Efimov three-body effects into account in the strong coupling regime [31]. The calculation assumes a large mass ratio $M \gg m$ and reproduces the RKKY potential in the weak interspecies interaction limit, and the Efimov potential in the limit of dilute Fermi gas. Here we summarize our calculation based on the paper.

Consider two Cs atoms separated by R is immersed in a Fermi gas, the effective potential between them $V(R)$ is derived in Eqs. (5-7) from Ref. [31]. We calculate the Cs-Cs scattering property from $V(R)$ with the variable phase equation, see Fig. S3. Pairing resonances occur when the scattering length flips sign.

The theory suggests a clear shift of the resonance position toward smaller interspecies scattering length a_{BF}

when fermion density increases. This confirms a stronger mediated attractions in a denser Fermi gas and thus a smaller interspecies scattering length can bind Cs atoms. In the opposite limit when the Fermi gas density approaches zero, we recover the Efimov resonance.

Finally we compare the boson binding length a_1 and fermion binding length a_2 . Fermions are bound to boson

pairs when the magnitude of the interspecies scattering length $|a_{\text{BF}}|$ exceeds the pair size of the pairs [31]. As k_{F} characterizes the length scale of the fermion mediated potential and thus the boson pair size. We obtain the condition to bind fermions as $|a_2| \approx k_{\text{F}}^{-1}$. Thus we conclude a much stronger attraction $|a_2| > |a_1|$ is needed to bind light fermions than heavy bosons, which is in full agreement with our observation.